Proceedings of the 7th International Conference on Asian and Pacific Coasts (APAC 2013) Bali, Indonesia, September 24-26, 2013

WINTERTIME EXTREME STORM WAVES IN THE EAST SEA (JAPAN SEA): NUMERICAL EXPERIEMTNS OF STORM WAVE OVERTOPPING IN THE FUSHIKI PORT, THE TOYAMA BAY

H.S. Lee [1], T. Komaguchi [2] and M. Hara [3]

ABSTRACT: In the winter East Sea (ES), storm waves due to winter storms (e.g. extratropical cyclones) under the context of the cold and dry East Asian winter monsoon are frequently reported causing extensive coastal damages along the coasts of Korea and Japan. In February 2008, abnormal storm waves due to a moving low propagating from the west off Hokkaido, Japan, to the south and southwest caused severe coastal damages along the Toyama Bay coast. In this study, we perform numerical experiments on wave overtopping and run-up in the Fushiki Port, Toyama Bay, where the long North-Breakwater was heavily damaged by the storm waves in February 2008. The experiments are conducted using an open-source Gerris flow solver (Gfs) based on modified non-linear shallow-water equation with adaptive mesh refinement (AMR) method and wet-dry scheme for the potential extreme storm waves of 6.78 m and 18.28 sec obtained from statistical analysis and wind wave modeling. The refined mesh efficiently resolves the complicated coastline and coastal structures in the Fushiki Port. The results show that the Fushiki Port would be overtopped and flooded by extreme storm waves if the North-Breakwater does not function properly after being damaged. Also the storm waves would overtop seawalls and sidewalls of the Manyou Pier behind the North-Breakwater. The results also depict that AMR method and wet-dry scheme capture the coastline and coastal structure very well while keeping the computational load efficiently.

Keywords: extratropical cyclone, storm waves, Fushiki Port, Toyama Bay, Gerris, adaptive mesh refinement.

INTRODUCTION

In the East Sea (ES) during winter, mean surface winds over the sea are northeasterly and generally strong due to two synoptic-scale features, the Siberian High and the Aleutian Low, under the context of the cold and dry East Asian winter monsoon. Storm waves due to winter storms (e.g. extratropical cyclones) in the winter ES are frequently reported causing extensive coastal damages along the coasts of Korea and Japan.

In February 2008, abnormal storm waves due to a developed low propagating from the west off Hokkaido to the south and southwest in the ES caused extensive damages along the coasts of Korea and Japan (Figure 1). The abnormal storm waves propagated into the Toyama Bay, Japan, caused one of the most severe coastal damages ever induced by such conditions. The observed maximum significant wave height and period at the Fushiki-Toyama buoy in the Toyama Bay are 4.22 m and 14.2 sec, respectively. Such abnormal waves are called "Yorimawari Waves" by the local people and investigated by Lee et al. (2010) on their generation mechanisms by thorough literature reviews and numerical experiments.

The Fushiki Port experienced large damages in its North-Breakwater due to the Yorimawari Waves. The storm waves were refracted by the local bathymetry, and then wave energies were concentrated on certain parts of the North-Breakwater, resulting in the damaged blocks (Figure 1).

In our accompanying paper in this volume (Lee et al., 2013), they investigate the extreme storm waves in the Toyama Bay based on statistical analysis and numerical modeling. Firstly, an extreme condition of the transition time of moving lows is estimated using extreme value method fitting to the Gumbel distribution. Secondly, an extreme condition for wind intensity is obtained from observed data analysis and empirical formula. Then, finally numerical experiments are conducted to evaluate the potential extreme storm waves in the Toyama Bay under the extreme conditions of wind intensity and duration obtained above using a non-hydrostatic meteorological model, WRF, and a wind wave model, WAVEWATCH III. The resulting significant wave

[1] Graduate School for International Development and Cooperation, Hiroshima University, 1-5-1 Kagamiyama, Higashi-Hiroshima 739-8529, Hiroshima, JAPAN
[2] Blue Wave Institute of Technology, Tokyo, JAPAN
[3] Idemitsu Engineering, Co., Ltd, JAPAN

height and period of the extreme storm waves at the Fushiki-Toyama are 6.78 m and 18.28 sec, respectively.

Therefore, the objective of the present study is to investigate the functionality of the North-Breakwater of the Fushiki Port and to examine if the current coastal structures of the Fushiki Port are durable against such extreme storm wave conditions or not.

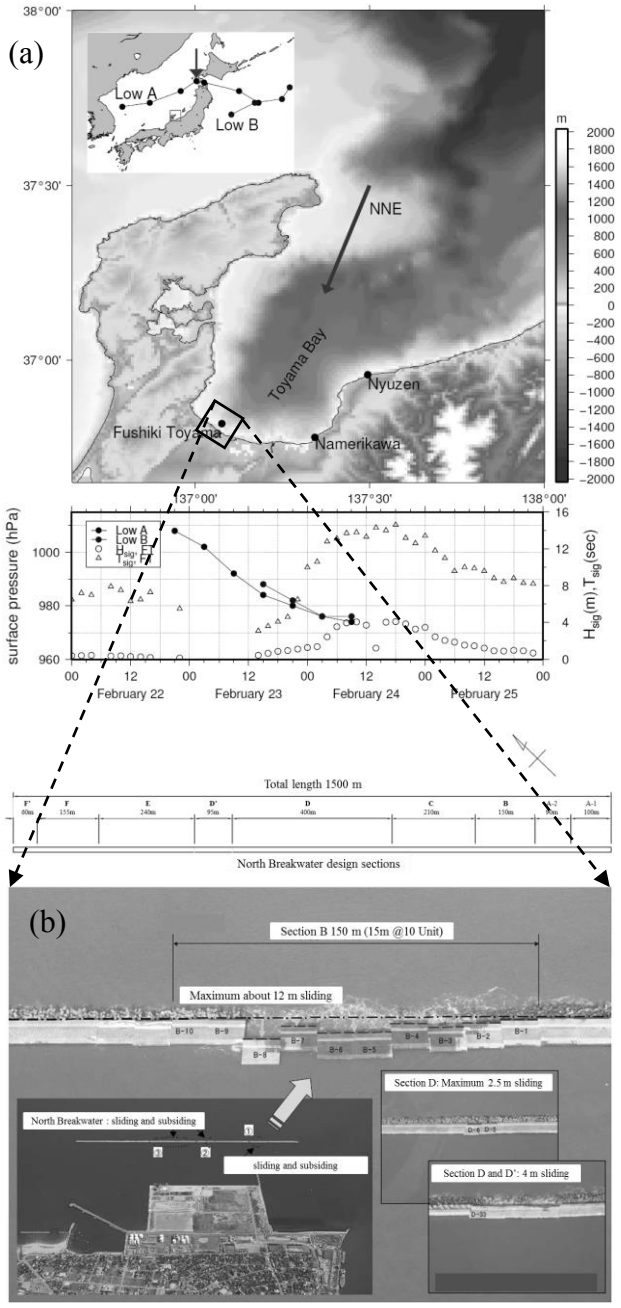

Fig. 1 (a) Tracks of low pressures and observed wave direction (upper panel) and the pressure variations of lows in time together with observed H_s and T_s at the Fushiki-Toyama buoy (lower panel) and (b) aerial images of the Fushiki Port and the damaged North-Breakwater

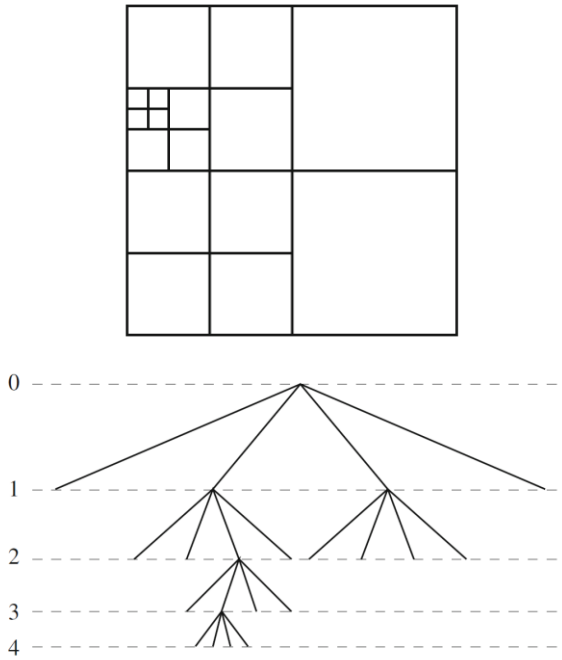

Fig. 2 Example of quadtree discretization (top) and its local representation together with the level of the cells in the tree (bottom)

DATA AND METHOD

The Fushiki Port and damage pattern

The Fushiki Port is located near the Fushiki-Toyama Buoy site with the 1500 m long North-Breakwater perpendicular to the NNE direction (Figure 1(a)). During the storm wave events in February 24 2008, the wave energies are focused on Sections B, D and D' of the breakwater due to the refraction of waves by local bathymetry. Therefore, the corresponding sections of the breakwater are damaged with maximum 12 m, 2.5 m, and 4 m sliding backward to the pier and the armors in front of the breakwater are subsided by the storm waves (Figure 1(b)). The storm waves of about 4 m are consistently propagated to the port more than 12 hrs.

Gerris flow solver (Gfs)

Gfs is an open source computational fluid dynamic code solving the non-linear shallow water equations. In this section, Gfs is described briefly in terms of the governing equations, the numerical scheme, and the adaptive mesh refinement method. Full details are referred to Popinet (2003; 2011).

Governing equations

Long waves such as tides and tsunamis are most commonly modelled using a longwave approximation of the mass and momentum conservation equations for a fluid with a free surface. In this approximation, the slopes of both the free surface and the bathymetry are

assumed to be vanishingly small. Note that these assumptions are often violated in the case of tsunamis, particularly close to shore, however and somewhat surprisingly, the long-wave approximation still gives reasonable results in practice. Simple scaling arguments show that the vertical velocity of the fluid is also vanishingly small in this context. Fluid motion can, thus, be described only using the vertically averaged components of the horizontal momentum and the free-surface elevation. The modified non-linear shallow water equations with a source term for Coriolis Effect can be described as

$$\frac{\partial h}{\partial t}+\frac{\partial}{\partial x}(hu)+\frac{\partial}{\partial y}(hv)=0 \tag{1}$$

$$\frac{\partial (hu)}{\partial t}+\frac{\partial}{\partial x}(hu^2+\frac{1}{2}gh^2)+\frac{\partial}{\partial y}(huv)-fv=-hg\frac{\partial z}{\partial x} \tag{2}$$

$$\frac{\partial (hv)}{\partial t}+\frac{\partial}{\partial u}(huv)+\frac{\partial}{\partial y}(hv^2+\frac{1}{2}gh^2)+fu=-hg\frac{\partial z}{\partial y} \tag{3}$$

where h is free surface elevation, $\boldsymbol{u}=(u, v)$ is the horizontal velocity vector, g is the acceleration due to gravity, z is the depth of bathymetry, and f is the Coriolis coefficient. An implicit scheme for quadratic bottom friction with the friction coefficient of 0.001 is also applied.

Numerical scheme

Numerical methods for hyperbolic systems of conservation laws have been extensively developed in the context of compressible gas dynamics with applications in aeronautics in particular. Many of these schemes are suitable for solving the Saint-Venant equations provided the following two important specificities are taken into account: the solver needs to properly account for vanishing fluid depths and needs to verify exactly the lake-at-rest equilibrium solution.

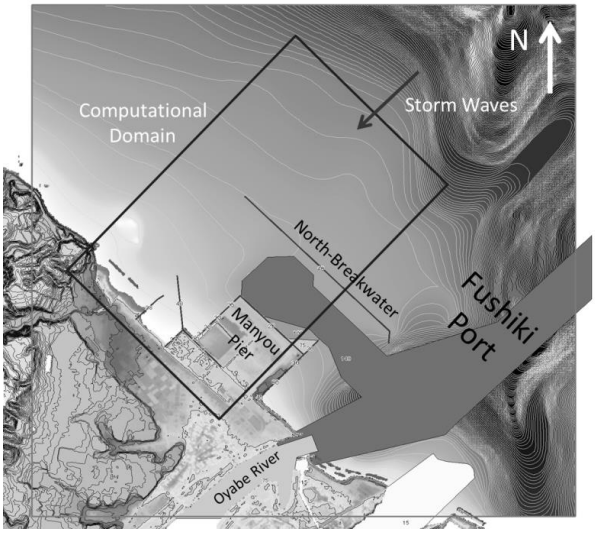

Fig. 3 Computational domain and bathymetry

The Saint-Venant solver used in Gfs is based on the numerical scheme analysed in detail by Audusse et al. (2004) which verifies both properties. The scheme uses a second-order, slope-limited Godunov discretization. The Riemann problem necessary to obtain Godunov fluxes is solved using an approximate Harten-Lax-van Leer Contact (HLLC) solver which guarantees positivity of the water depth. The choice of slope limiter is important as it controls the amount of numerical dissipation required to stabilize the solution close to discontinuities. Following Popinet (2011), the Sweby limiter is a good comprise between stability of short waves and low dissipation of long waves. A MUSCL-type discretization is used to generalize the method to second-order timestepping. The time-step is constrained by the Courant-Friedrich-Levy condition for stability as

$$\Delta t<\frac{1}{2}\min(\frac{\Delta}{|u|+\sqrt{gh}}) \tag{4}$$

where Δ is the mesh size.

To summarize, the overall scheme is second-order accurate in space and time, preserves the positivity of the water depth and the lake-at-rest condition and is volume- and momentum-conserving.

Adaptive mesh refinement

Gfs uses a quadtree spatial discretization which allows efficient adaptive mesh refinement. An example of the quadtree structure is exhibited in Figure 2 together with its logical (tree) representation. This tree can be conveniently described as a “family tree” where each parent cell can have zero or four children cells.

An important parameter is the level of a given cell in the tree. The root cell has level zero by convention and the level increases by one for each successive generation in the tree. A further simplification is obtained by constraining the quadtree so that the level of adjacent cells cannot differ by more than one. This reduces the number of configurations for neighbouring cells to two: (1) neighbouring cells are on the same level: this is identical to a regular Cartesian grid discretization. (2) Two fine cells are neighbouring the same coarse cell.

In order to refine or coarsen the mesh dynamically, one needs to choose a refinement criterion. This choice is not trivial and depends on both the details of the numerical scheme which control how discretization errors and the physics of the problem considered which control how discretization errors will influence the accuracy of the solution. Gfs provides a variety of refinement criteria which can be flexibly combined depending on the problem. In this study, the gradient of free surface elevation was used for the refinement criterion. Cells also need to be coarsened, for example their children are destroyed, when a high spatial

resolution is not required anymore. Cells cannot be refined/coarsened between successive time-steps. When cells are coarsened, the values of fields are set by defaults to the averages over their children, which also ensure conservation of quantities.

Numerical experiments

Numerical experiments are carried out with three different configurations of the North-Breakwater to investigate its functionality against the extreme storm waves. Figure 3 shows the computational domain in meter (2500 m × 1500 m) and the ambient bathymetry of the Fushiki Port.

Table 1 Configurations of numerical experiments for wave overtopping and run-up using Gfs.

Run	Breakwater	Length (m)	Damaged sections
CB	No damages	1,500	No
DB	Damaged	910	DD'EF
NoB	No-breakwater	0	All

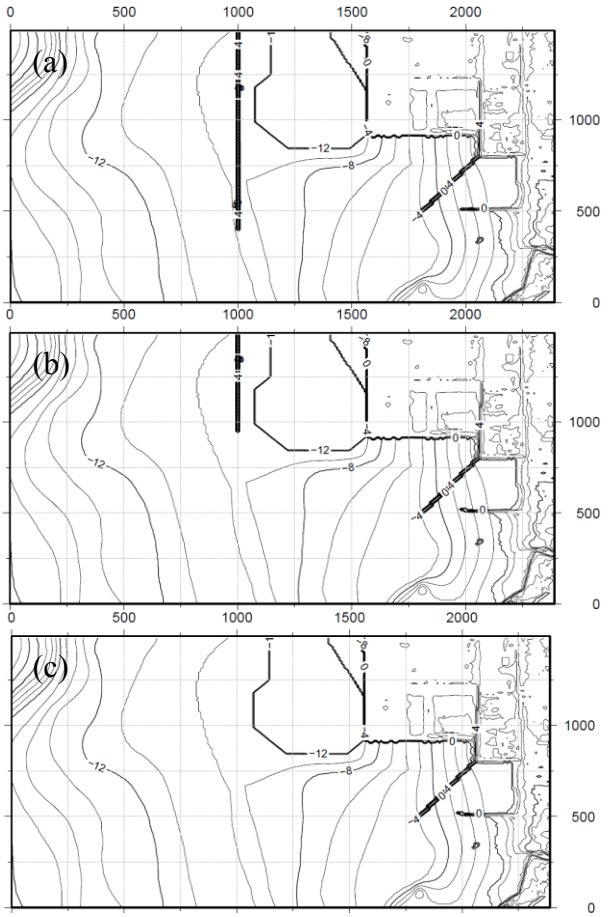

Fig. 4 Configurations of the North-Breakwater for three experiments together with local bathymetry, (a) CB, (b) DB, and (c) NoB.

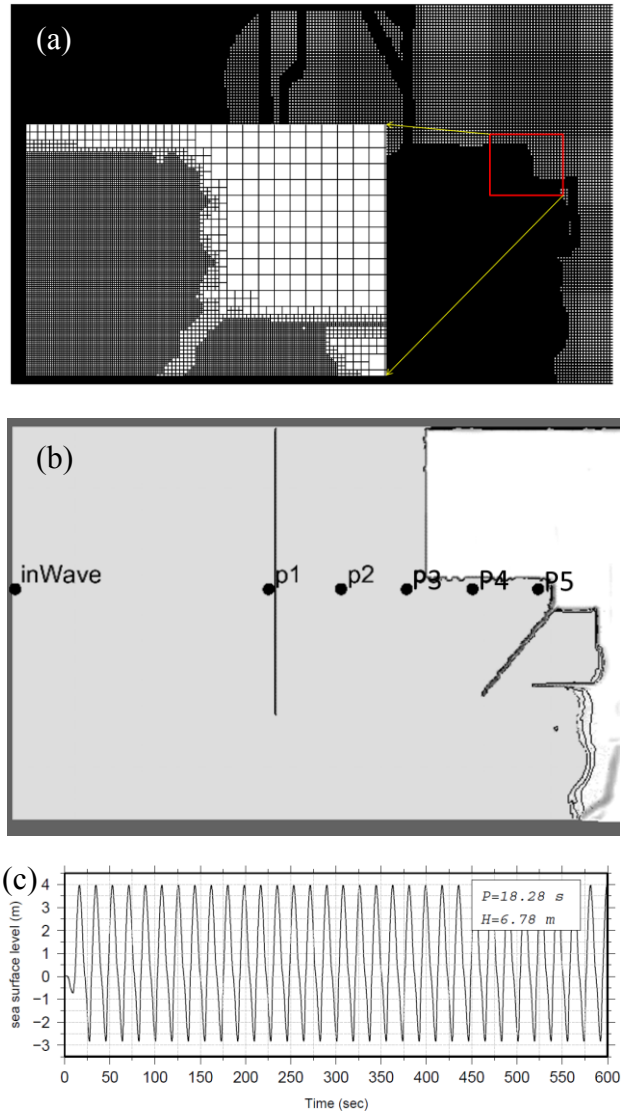

Fig. 5 (a) The initial mesh, (b) locations of six probes, and (c) temporal profile of the incident waves.

In front of the breakwater, the bathymetry changes rapidly and the water depth between the North-Breakwater and the Manyou Pier is dredged for navigational and shipping purpose. The dredged channel is extended to the mouth of Oyabe River. Figure 4 illustrates the three configurations of the breakwater with water depth: (a) the current condition with full functionality (CB), (b) a damaged condition with partial functionality (DB), (c) no-breakwater condition with no functionality (NoB). Table 1 also displays the details of the breakwater configurations for the experiments.

In Figure 5(a), the initial mesh is presented illustrating the different levels of meshes depending on the local bathymetry and topography. Within the computational domain, six probes are defined to investigate the flow characteristics as illustrated in Figure 5(b). The first probe is located just after the incident wave inputs, the second one is positioned just before the North-Breakwater, and the followings are

positioned in line from left to right with the last probe placed just before the seawall in front of triangle focusing point. The incident wave profile is also displayed in Figure 5(c) with wave height of 6.78 m and wave period of 18.28 sec in the perpendicular direction to the North-Breakwater. The two lateral sides are applied to a radiation boundary condition letting the waves freely out.

RESULTS

Figure 6 shows the sea level variations in time from the three experiments at Probe 5. Firstly, the role of the North-Breakwater can be found at the arrival time of the first wave. With the current North-Breakwater, the first wave arrives after 200 sec, while, in other results, the first waves appear before 200 sec.

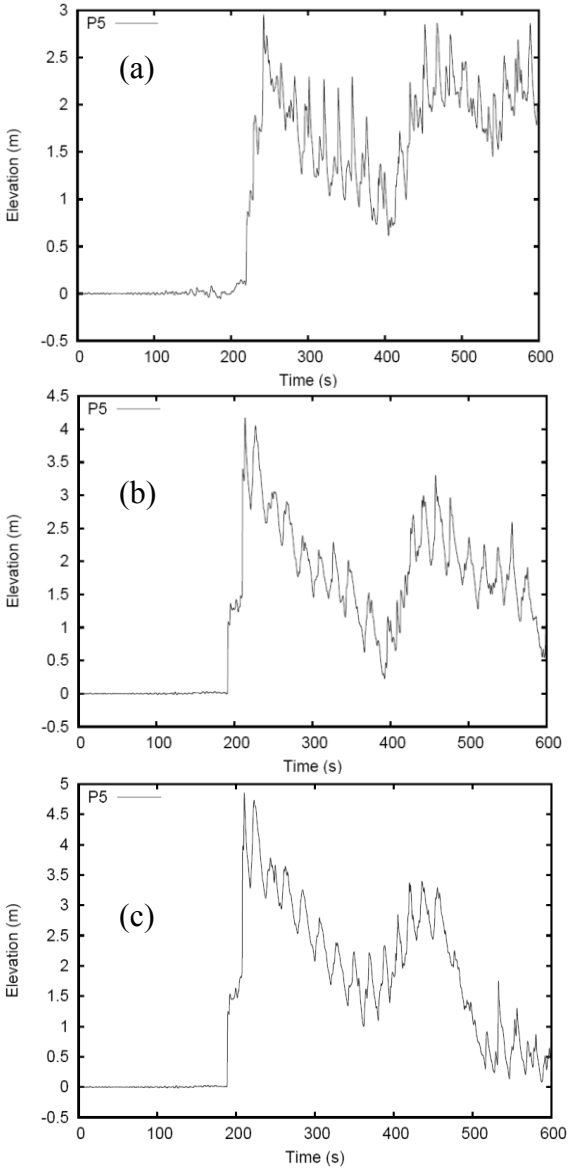

Fig. 6 (a) The initial mesh, (b) locations of six probes, and (c) temporal profile of the incident waves.

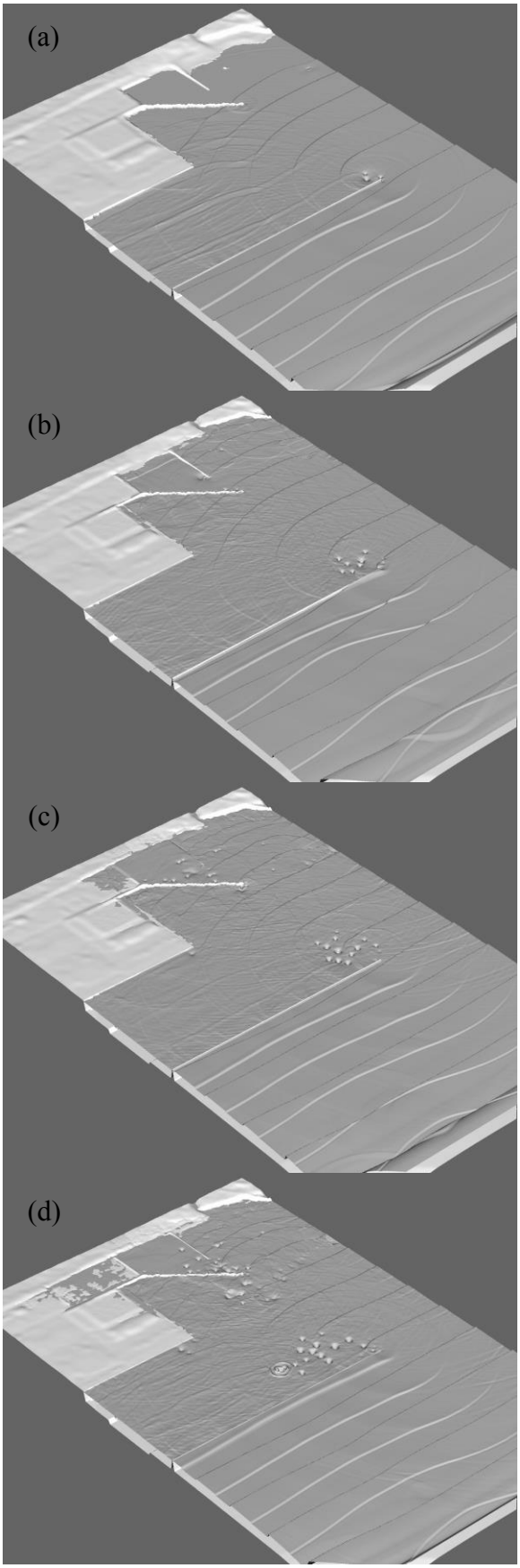

Fig. 7 3D snapshots of sea level variations from the CB experiment at (a) 180 sec, (b) 300 sec, (c) 420 sec, and (d) 540 sec after the start of simulation.

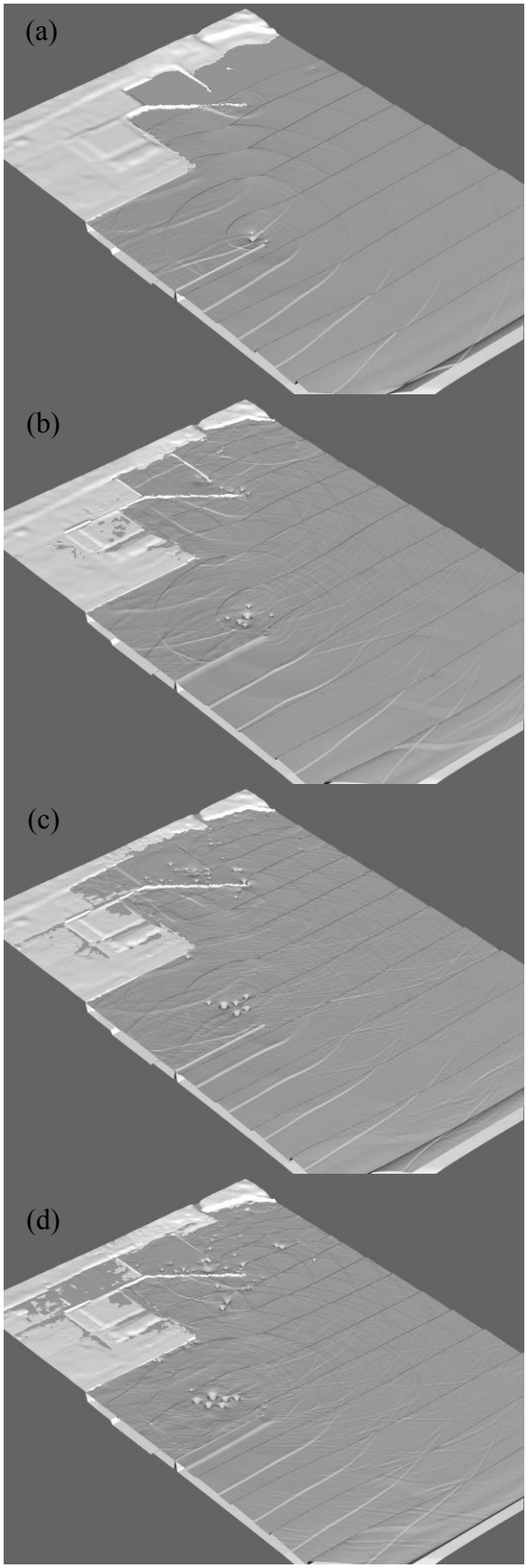

Fig. 8 3D snapshots of sea level variations from the DB run at (a) 180 sec, (b) 300 sec, (c) 420 sec, and (d) 540 sec after the start of simulation.

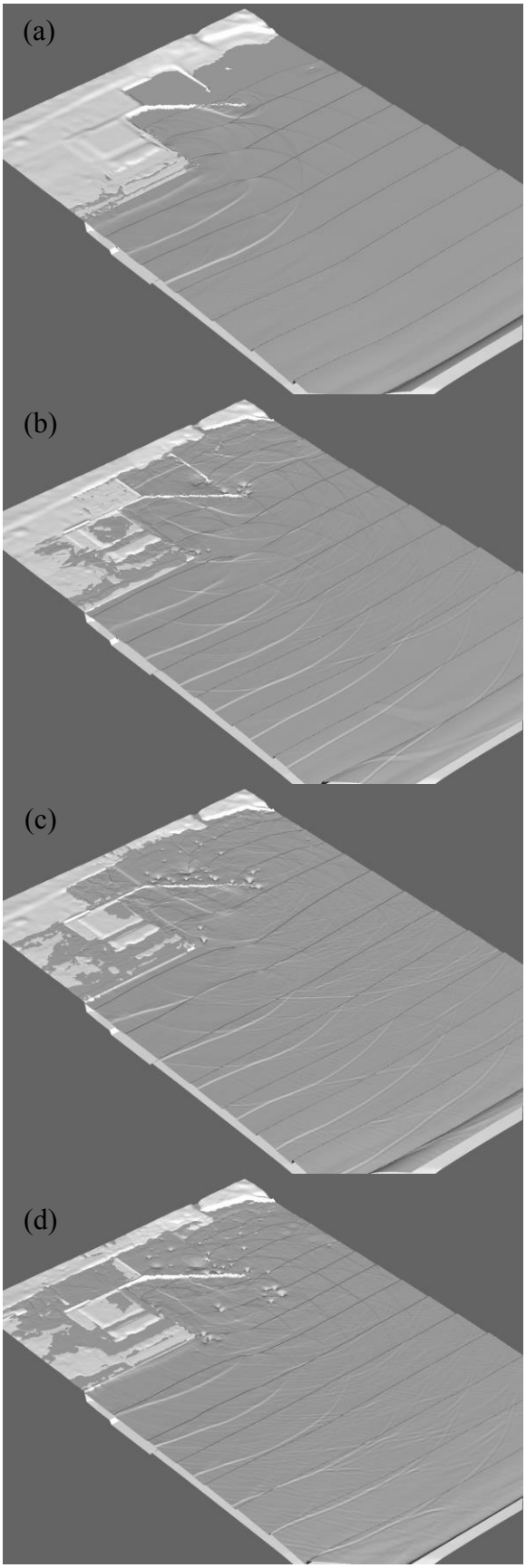

Fig. 9 3D snapshots of sea level variations from the NoB experiment at (a) 180 sec, (b) 300 sec, (c) 420 sec, and (d) 540 sec after the start of simulation.

In the CB experiment's result, the maximum water level appears to be less than 3 m by the first arrival. Then, the water level decreases gradually down to the minimum value at about 400 sec exhibiting the water level modulation due to the interaction of incoming and reflected waves between the maximum and minimum water levels. Then, the second and third peaks of water level appear at about 460 and 600 sec in the CB run. In the DB experiment, the first wave arrives just before 200 sec and the maximum water level increases over 4 m. The minimum water level within the result appears before 400 sec earlier than the CB result. Interestingly, after the second peak at about 450 sec, water level modulation becomes larger than the modulation between the maximum and minimum water levels from 200 to 400 sec. In the NoB results, the first wave arrives slightly earlier than the DB case and the maximum water level reaches nearly 5 m before 200 sec. The minimum water level is also presented earlier that the other runs at about 360 sec with about 1 m, which is the highest value among the experiments. Noticeably, after the second peak at about 440 sec, the water level depicts smooth drops compared to the other runs, resulting from the large overtopping of waves.

Figures 7 to 9 illustrate the 3D snapshots of sea level variations. In the CB results of Figure 7, the role of the North-Breakwater is clearly presented that the front of Manyou Pier is not overtopped due to the North-Breakwater. However, the Manyou Pier is overtopped from the side-seawall where the Probe 4 and 5 are positioned. Since the height of side-seawall of the Manyou Pier is gradually decreasing, the side-seawall overtopping is visible after 300 sec. In addition, the heavy overtopping in the inner Manyou Pier is outstanding from the side-seawall next to the small port formed by the oblique breakwater in the left of Probe 5 and groyne. One of the outstanding features by using the adaptive mesh is the small vortices formed by diffraction and interactions of waves near the edge of breakwaters. However, since the non-linear shallow water equations do not include the viscous term, the vortices keep their motions without turbulent and viscous dissipations.

The wet-dry scheme together with adaptive meshes is able to model the run-up and capture the shoreline changes well and efficiently depending on flow features, which is the free surface gradient in this study.

Figure 8 exhibits the 3D snapshot of sea level variations from the DB run, which considers the partial damage of the North-Breakwater. It is illustrated at the snapshot at 180 sec that the first wave arrives faster than the CB run. The overtopping from the side-seawall occurs earlier in time and larger in volume than the CB run. Also the overtopping over the side-seawall from the small port becomes severer and the inner Manyou Pier is heavily flooded. Small vortices are also observed in the DB results. An overtopping over the front seawall is not observed in the DB run.

Figure 9 represents the 3D snapshots from the no breakwater case, the NoB run, at 180, 300, 420 and 540 sec after the simulation starts. The first wave arrival is depicted at the 180-sec snapshot and the front seawall of the Manyou Pier is visible at this time step. The Manyou Pier experiences complete flooding from the front and side seawall. The small port next to the inner Manyou Pier is totally packed with sea water. A number of small vortices are also observed near the oblique breakwater.

CONCLUSIONS

In the winter East Sea, coastal damages and disasters in Korean and Japanese coasts are often occurred by storm waves due to rapidly developing low pressure systems. In February 2008, storm waves due to a moving low propagating from the west off Hokkaido, Japan, to the south and southwest caused severe coastal damages along the Toyama Bay coast. In particular, the Fushiki Port in the Toyama Bay experienced severe damage in its North-Breakwater which protects the Manyou Pier behind in the south.

The current study investigates the functionality of the North-Breakwater in the Fushiki Port, the Toyama Bay against the extreme storm waves due to storms and extratropical cyclones. The extreme storm waves with Hs of 6.78 m and Ts of 18.28 sec are estimated by statistical analysis and numerical experiments described in the accompanying paper in this volume.

Numerical experiments using a modified non-linear shallow water equation model with adaptive mesh refinement method are carried out to investigate the North-Breakwater functionality. Three experiments are considered for current, damaged and no breakwater cases. In all runs, the inner Manyou Pier becomes overtopped over the side seawall adjacent to a small port formed by breakwater and groyne. The North-Breakwater is proved to be a protector for the Manyou Pier from overtopping over the front seawall. It also affects the maximum water level and arrival time of the first wave.

In this numerical experiment, however, there are a couple of limitations as follows. Firstly, the functionality of the North-Breakwater is not directly and explicitly considered in the simulation. Therefore, it is unknown that if the North-Breakwater itself would be damaged, for example, sliding or overturning due to the extreme storm waves. Secondly, the temporal profile of the incident waves at the open boundary does represent a series of sinusoidal waves with wave height of 6.78 m and wave period of 18.28 sec rather than representing

wave characteristics with Hs and Ts of wave groups or wave trains.

Lastly, according to the linear wave theory, the wavelength of the incoming storm waves is over 500 m, given the wave height of 6.78 m and period of 18.28 sec and average depth of the Toyama Bay of 400 ~ 500 m. Meanwhile, the water depth in the computational domain is less than 20 m. Therefore, the ratio between the wavelength (λ) and the water depth (h) are larger than 20, which fall into the conventional shallow water criterion. Therefore, it can be stated that the long wave approximation is still valid in this study. However, considering the second limitation, it is favorable to use the KdV equations or Boussinesq equations for wide range applications.

Therefore, those limitations have to be considered when interpreting the simulation results of this study and have to be improved in further works.

ACKNOWLEDGEMENTS

This study is supported by the Grant-in-Aid Young Scientist (B) of MEXT.

REFERENCES

Audusse, E., Bouchut, F., Bristeau, M.-O., Klein, R. and Perthame, B. (2004). A fast and stable well-balanced scheme with hydrostatic reconstruction for shallow water flows. SIAM J. Sci. Comput. 25(6): 2050-2065.

Lee, H.S., Kim, K.O., Yamashita, T., Komaguchi, T. and Mishima, T. (2010). Abnormal storm waves in the winter east/japan sea: Generation process and hindcasting using an atmosphere-wind wave modelling system. Nat. Hazards Earth Syst. Sci. 10(4): 773-792.

Lee, H.S., Komaguchi, T. and Yamamoto, A. (2013). Wintertime extreme storm waves in the East Sea: Estimation of extreme storm waves in the Toyama Bay, Japan. Proceedings of the 7th International Conference on Asian Pacific Coasts (APAC2013), Bali, Indonesia.

Popinet, S. (2003). Gerris: A tree-based adaptive solver for the incompressible euler equations in complex geometries. Journal of Computational Physics. 190(2): 572-600.

Popinet, S. (2011). Quadtree-adaptive tsunami modelling. Ocean Dynamics. 61(9): 1261-1285.